An investigation of Vulcanian eruption dynamics using laboratory analogue experiments and scaling analysis

A. B. CLARKE[1]*, J. C. PHILLIPS[2] & K. N. CHOJNICKI[1]

[1]*School of Earth and Space Exploration, Arizona State University, Tempe, AZ, 85287–1404, USA*

[2]*Center for Environmental and Geophysical Flows, Department of Earth Sciences, University of Bristol, Wills Memorial Building, Queen's Road, Bristol, BS8 1RJ, UK*

**Corresponding author (e-mail: amanda.clarke@asu.edu)*

Astract: Vulcanian eruptions are frequent, small-scale, short-lived explosive volcanic eruptions, which are thought to be produced by impulsive sources. The experiments presented here, produced by injections of mixtures of water, alcohol or salt and solid particles into fresh water, created a wide variety of turbulent flows from steady and impulsive sources. We focus on the experimental flows analogous to Vulcanian events – unsteady, finite-volume releases of buoyancy (thermals) and momentum (puffs), and short releases driven by both momentum and buoyancy. Dimensional analysis, based on two controlling source parameters, total injected momentum (M) and total injected buoyancy (B), identified a universal scaling relationship for the propagation of the flows; the non-dimensional, time-varying velocity term ($ut^{1/2}/B^{1/4}$), where u is flow front vertical velocity and t is time from flow onset, varies with the time-varying, non-dimensional ratio of source parameters (M/Bt), such that $ut^{1/2}/B^{1/4} = k(M/Bt)^{1/2}$. The quantitative relationship successfully describes experiments and several Vulcanian eruptions for a wide range of initial conditions. The utility of the relationship is demonstrated by estimating total mass erupted and vent mass flux as a function of time, two parameters important to hazards assessment, for the well-documented 7 August 1997 Vulcanian eruption at Soufrière Hills volcano, Montserrat. Results compare favourably to independent estimates of total mass erupted (based in part on deposit studies) and eruption duration (based on seismic analysis) with the advantage that our approach requires only the determination of the eruption cloud front velocity from conventional video analysis.

Particle-laden jets and plumes occur in many environments and settings, including atmospheric clouds (Turner 1966), black smokers at mid-ocean ridges (Sudarikov & Roumiantsev 2000), rivers entering bodies of water (Cookman *et al.* 1997), industrial explosions and smokestacks, bomb and meteorite impact zones, fuel injectors (Lee *et al.* 2004) and volcanic eruptions (Sparks *et al.* 1997). In most cases, they are generated by unsteady source flux, but unfortunately there is little fundamental understanding of how to relate time-varying and impulsive source fluxes to flow evolution, and no complete theoretical description which does so over a wide range of conditions.

This work focuses on the specific case of hazardous Vulcanian eruptions, which are generated by highly unsteady, short-lived vent fluxes of momentum and/or buoyancy. Vulcanian eruptions are generally characterized as discrete, violent explosions which are generated by an impulsive source (Morrissey & Mastin 2000). Often they result from a sudden decompression of a conduit containing pressurized, vesiculated magma (Self *et al.* 1979; Woods 1995; Sparks *et al.* 1997; Stix *et al.* 1997; Druitt *et al.* 2002). Such eruptions have been described in detail at a number of volcanoes (Sparks *et al.* 1997), including Ngauruhoe, New Zealand (Nairn & Self 1978; Self *et al.* 1979), Galeras, Colombia (Stix *et al.* 1997), and Soufrière Hills volcano, Montserrat (Druitt *et al.* 2002). Typically only a portion of the magma in the conduit is fragmented and evacuated, such that Vulcanian eruptions last only seconds to minutes and erupt less than 0.1 km^3 of magma (Morrissey & Mastin 2000). Vulcanian explosions can produce atmospheric shock waves (Nairn 1976; Ishihara 1985), exhibit vent velocities up to hundreds of metres per second, eject blocks and bombs up to 5 km from the vent (Fagents & Wilson 1993; Waitt *et al.* 1995; Druitt *et al.* 2002) and can produce vertical turbulent plumes up to 20 km high (Morrissey & Mastin 2000).

The short-duration, unsteady nature of Vulcanian eruptions makes them distinct from Plinian eruptions, in which it is generally accepted that bubbly magma rises to meet a fragmentation wave, and, as is commonly assumed, steadily feeds the vent flux over long periods. However, most Plinian

From: THORDARSON, T., SELF, S., LARSEN, G., ROWLAND, S. K. & HOSKULDSSON, A. (eds)
Studies in Volcanology: The Legacy of George Walker. Special Publications of IAVCEI. **2**, 155–166.
Geological Society, London. 1750-8207/09/$15.00 © IAVCEI 2009.

eruptions exhibit temporal variations associated with changes in vent mass flux (e.g. Carey & Sigurdsson 1987; Scott *et al.* 1996; Sparks *et al.* 1997; Di Muro *et al.* 2004; Houghton *et al.* 2004), making existing steady jet and plume theory approximate at best (e.g. Turner 1973) for both Vulcanian and Plinian eruptions.

Vent mass flux for explosive volcanic eruptions is often estimated from column heights by assuming steady vent conditions (Wilson *et al.* 1980, following Morton *et al.* 1956) or by assuming that short-duration events are generated by an instantaneous, purely buoyant release (thermals; as summarized in Turner 1973, pp. 186–189). However, fundamental theory relating overall flow evolution to vent flux does not exist for short-lived highly unsteady momentum- and buoyancy-driven releases, and therefore there is no simple means of estimating time-varying mass flux or total mass erupted by short-duration explosive events. Our preliminary calculations suggest that over long episodes of periodic eruptive activity (such as at Santiaguito volcano in Guatemala), the total mass erupted by Vulcanian eruptions could be large, and is therefore worth quantifying. Santiaguito has been producing periodic explosive eruptions since the 1970s (e.g. Rose 1980; Johnson *et al.* 2004). We can conservatively estimate the mass erupted at Santiaguito by assuming that 10^4 m^3 dense rock equivalent (DRE $= 2500$ kg m^{-3}), which is equivalent to 2.5×10^7 kg of magma, was erupted 10 times a day over 20 years, resulting in a total of 1.9×10^{12} kg. For comparison, the Plinian phase of the Mount Pinatubo eruption in 1991 ejected roughly 1.3×10^{13} kg of magma (Scott *et al.* 1996). In contrast to many Plinian eruptions, the ash erupted by Santiaguito volcano is not ejected into the stratosphere where it may potentially have a global affect, but the mass erupted is significant and can have devastating effects on local crops and nearby populations.

In this paper we present a laboratory investigation of the fundamental dynamics governing short-duration, unsteady, turbulent flows for which both buoyancy and momentum may be important. We varied buoyancy and momentum injected in order to develop a scaling analysis that enables our experiments to be compared with Vulcanian eruptions. The experimental method is described first, followed by qualitative observations and general experimental results. Dimensional analysis is then used to develop a scaling relationship for the laboratory experiments. We then demonstrate that the same scaling relationship describes several well-documented Vulcanian eruptions. Finally, inspired by George Walker's pioneering approach of using quantitative estimates based on field observations to infer controlling parameters for volcanic processes, we extract a simple formula from the dimensional analysis in order to estimate the mass flux and mass erupted by Vulcanian events using direct observations of the rise rate of the eruption column. The paper concludes with recommendations for future field measurements that are required for further development of predictive models of Vulcanian eruptions.

Methods

High-pressure suspensions of particles in aqueous solution were rapidly released into a tank of fresh water in a series of systematic laboratory experiments. The injected volume, buoyancy, momentum, particle size and concentration were varied to produce a range of flows. Flow types included *plumes* (steady releases where only buoyancy controls the flow propagation), *jets* (steady releases where only momentum controls the flow propagation), *thermals* (impulsive releases where only buoyancy controls the flow propagation), *puffs* (impulsive releases where only momentum controls the flow propagation) and *collapsing fountains* which generated density currents. This paper focuses solely on the impulsive releases (thermals, puffs and releases driven by both momentum and buoyancy) as analogous to flows produced by Vulcanian eruptions.

A schematic of the experimental apparatus is shown in Figure 1. The reservoir was filled with a

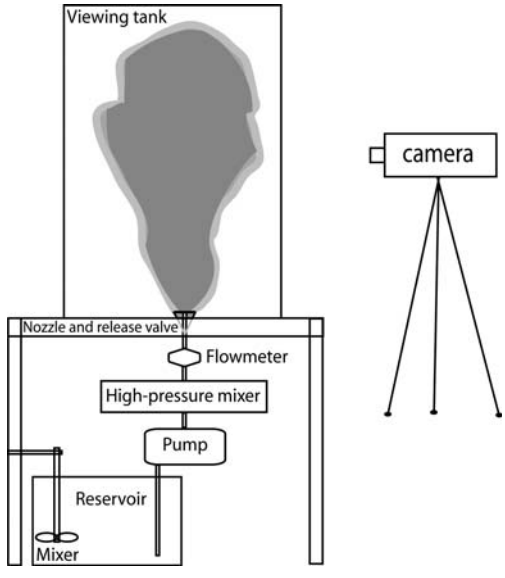

Fig. 1. Schematic, not-to-scale, drawing of the experimental setup. The Lexan viewing tank had base dimensions of 0.61 by 0.61 m and was filled to a depth of 1 m with fresh water.

mixture of either water and isopropyl alcohol with or without solid particles, or water and salt with or without solid particles. The particles were either <10 μm diameter silica powder (Sigma Chemical Company) or 45 μm diameter glass Ballotini spheres (Potters Inc.), both with density of 2500 kg m^{-3}. Particle concentration was varied systematically up to 3.5 vol%. The reservoir was pressurized up to 23 MPa with a Graco Ultra 395 high-pressure paint pump. Particles were kept in suspension prior to pressurization by a rotary mixer in the initial reservoir. A second, sealed, high-pressure mixing mechanism (rocking agitator) was installed between the pump and the flow metre for experiments with large (45 μm) particles, in order to prevent settling between the pump and release valve. Using a high-pressure ball valve, the particle suspension was rapidly released through a nozzle at the base of a Lexan viewing tank containing fresh water (Fig. 1). The volume and duration of the subsequent flow was not pre-determined but was limited by the potential energy associated with the pressurized fluid rather than by the volume of available fluid. The tank has base dimensions of 0.61 by 0.61 m and was filled to a depth of 1 m with fresh water.

The final exit of the nozzle consisted of interchangeable aluminium plates with circular holes of 3–15 mm in diameter which enabled the initial momentum of the release to be varied independently of the initial buoyancy and reservoir pressure. The effect of nozzle diameter on entrainment is generally insignificant; whether entrainment is described as being directly proportional to the local velocity scale in the flow (Morton *et al.* 1956) or is parameterized as a function of the Richardson number (which is also related to the local velocity scale; Kaminski *et al.* 2005), the effect of the nozzle diameter is very small because typically the region over which the nozzle sets the velocity scale is very small. The ratio of particle diameter to vent diameter ranged from 10^{-5} to 10^{-3}, while ratios for explosive volcanic eruptions can reach 10^{-8}.

The reduced gravity of the suspension, defined as

$$g' = g\left|\frac{\rho_f - \rho_a}{\rho_a}\right| \quad (1)$$

where ρ_f is the density of the injected fluid and ρ_a is the density of the ambient fluid in the tank, was varied from 0 to ± 0.6 m s^{-2} using different proportions of water, isopropyl alcohol, salt and particles (the full range of experimental conditions is shown in Table 1). The reduced gravity of the laboratory experiments falls within (but does not cover) the range expected for Vulcanian eruptions. Sparks & Wilson (1982) suggested a value of 1.8 m s^{-2}, corresponding to an eruptive fluid density of 1 kg m^{-3}, although values ranging from 0 m s^{-2} to several hundred metres per second squared are reasonable, corresponding to fluid densities less than 1.225 kg m^{-3} to tens of kilograms per metre cubed (Wohletz 2001).

Mass flux at the vent was measured using an in-line Coriolis flow meter (Kueppers Elektromechanik; model KCM 3000-0-ND-FT-2) sampling at 100 Hz, allowing short duration, rapidly varying volume, buoyancy and momentum fluxes to be measured. In all experiments, the duration of the source injection (typically less than 1 s) was shorter than the observed life of the flows such that the ratio of the flow duration to injection duration ranged from 3 to 12. Total volume injected was calculated by integrating under the mass flow rate curve and dividing by fluid density (see example of mass flow rate curve in Fig. 2). The total volume injected was small compared with both the volume of the supplying reservoir and the volume required to occupy the plumbing system between the reservoir and the viewing tank, therefore the volume change of the reservoir was an unreliable means of estimating the volume of fluid which participated in a single experiment. More specifically, the total volume of fluid injected per experiment ranged from 15 to 180 cm^3 (15×10^{-6} to 180×10^{-6} m^3), and the volume of the supplying reservoir was on the order of 10 000 cm^3 (0.01 m^3), more than an order of magnitude greater. Furthermore, the total volume injected by each experiment was very small compared with the volume of the viewing tank (*c.* 0.37 m^3), thus measuring the change in fluid volume in the viewing tank also introduced a large amount of uncertainty.

Flow front propagation was recorded using high-speed video (Redlake © Motionscope MotionPro 2000) at rates up to 60 frames per second, and flow front velocities were obtained by scaled image analysis. Redlake © Midas software was used to spatially calibrate the experiment video from known dimensions in each image and to determine the maximum vertical position of the flow front in each frame of the video. The flow velocity was then calculated from the change in maximum vertical position between frames divided by the time interval between frames (1/60 s). This typically involved tracking the same lobe of the flow front throughout the experiment. However, large-scale turbulent eddies sometimes caused a different part of the plume to propagate ahead of the front that was being tracked, resulting in sudden changes in maximum vertical position, which contributed to fluctuations in the velocity.

Table 1. *Experiment details*

Experiment name	Symbol *In Figure 4*	Injected fluid density (kg* m^{-3})	Nozzle diameter (mm)	Reservoir pressure (psi)	Particle size (μm)	Particle concentration (vol% except where noted)	g' ($m^* s^{-2}$)	Volume, V (m^3)	Momentum, M ($m^4 s^{-1}$)	Buoyancy, B ($m^4 s^{-2}$)
6020604	◁	986	3	755	n/a	n/a	0.736	1.5500×10^{-5}	6.0700×10^{-5}	1.9800×10^{-6}
2402062c	•	962	3	2933	n/a	n/a	0.363	1.2610×10^{-4}	6.6190×10^{-4}	4.5820×10^{-5}
2402065	■	1028	3	764	n/a	0.0485 wt%	−0.285	2.0000×10^{-5}	7.1100×10^{-5}	5.6900×10^{-6}
2402066	◆	1028	3	2911	n/a	0.0485 wt%	−0.285	1.0160×10^{-4}	4.2430×10^{-4}	2.8930×10^{-5}
2702062	◀	964	15	790	<10	2	0.344	2.4700×10^{-5}	1.7200×10^{-5}	8.4900×10^{-6}
2802061b	☆	970	3	783	<10	2	0.285	2.5900×10^{-5}	1.3070×10^{-4}	7.3900×10^{-6}
2802062	■	970	3	2997	<10	2	0.285	1.4510×10^{-4}	8.7810×10^{-4}	4.1310×10^{-5}
2802063	◆	1035	3	791	<10	2	−0.354	4.5800×10^{-5}	2.1520×10^{-4}	1.3050×10^{-5}
2802064	▼	1035	3	2992	<10	2	−0.354	8.0300×10^{-5}	4.5900×10^{-4}	2.2870×10^{-5}
103063	◇	1035	3	793	<10	3.5	−0.354	4.9600×10^{-5}	2.2280×10^{-4}	1.7540×10^{-5}
103064	□	1035	3	2992	<10	3.5	−0.354	1.3610×10^{-4}	8.6820×10^{-4}	4.8120×10^{-5}
103065	×	1035	3	794	<10	3.5	−0.354	3.8000×10^{-5}	1.5900×10^{-4}	1.3450×10^{-5}
103066	*	1035	3	3011	<10	3.5	−0.354	6.9600×10^{-5}	4.3180×10^{-4}	2.4620×10^{-5}
103068	○	1035	15	2998	<10	3.5	−0.354	1.0500×10^{-4}	4.5160×10^{-4}	3.7140×10^{-5}
203061	+	962	15	750	~45	2	0.363	3.0200×10^{-5}	6.6200×10^{-5}	1.0970×10^{-5}
203063	☆	962	3	715	~45	2	0.363	5.0700×10^{-5}	3.4200×10^{-4}	1.8410×10^{-5}
203065	◁	1037	3	790	~45	2	−0.373	4.6200×10^{-5}	2.2320×10^{-4}	1.6330×10^{-5}
203066	▷	1035	3	2663	~45	2	−0.354	5.2900×10^{-5}	2.8480×10^{-4}	1.8710×10^{-5}
203067	△	1035	15	787	~45	2	−0.354	5.3700×10^{-5}	6.0400×10^{-5}	1.8980×10^{-5}
203069	◇	1037	15	644	~45	3.5	−0.373	1.0450×10^{-4}	1.7680×10^{-4}	3.8980×10^{-5}
2030611	□	1037	3	802	~45	3.5	−0.373	5.5900×10^{-5}	2.7800×10^{-4}	2.0880×10^{-5}
2030612	×	1037	3	2927	~45	3.5	−0.373	6.1100×10^{-5}	3.8760×10^{-4}	2.2810×10^{-5}
2030613	*	961	3	760	~45	3.5	0.373	1.9100×10^{-5}	1.0240×10^{-4}	7.1100×10^{-6}
2030614	○	961	3	3071	~45	3.5	0.373	1.8200×10^{-5}	1.0370×10^{-4}	6.7900×10^{-6}
2030615	+	961	15	671	~45	3.5	0.373	6.8600×10^{-5}	7.3500×10^{-5}	2.5590×10^{-5}
	In Figure 5									
mom3b	☆	999	15	2790	n/a	n/a	0.000	3.3470×10^{-5}	7.3200×10^{-5}	0.000
mom5	▽	999	15	2900	n/a	n/a	0.000	3.1190×10^{-5}	6.4000×10^{-5}	0.000
mom9	●	999	3	2840	n/a	n/a	0.000	2.1830×10^{-5}	1.9800×10^{-4}	0.000
moml0	■	999	3	1090	n/a	n/a	0.000	1.1380×10^{-5}	6.5000×10^{-5}	0.000

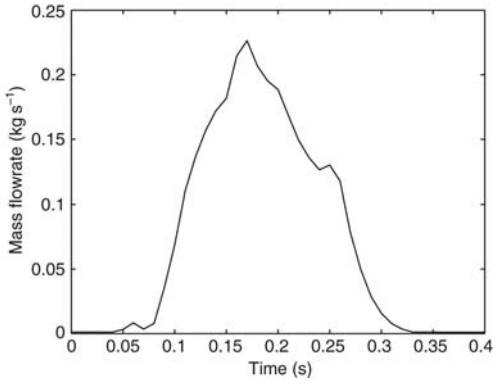

Fig. 2. Mass flow rate v. time for Experiment 2030611. Total mass injected for each experiment was calculated by integrating the area under the curve. Total volume injected was then calculated by dividing total mass injected by the fluid density. In this case, the volume injected was 5.59×10^{-5} m^3.

Experimental results

Variation of the experimental parameters produced a wide range of flows as described above, and field-documented Vulcanian explosions exhibit this same wide range of behavior (e.g. Self *et al.* 1979; Sparks & Wilson 1982; Clarke *et al.* 2002, Druitt *et al.* 2002). Our experiments produced flows that were fully turbulent, with Reynolds numbers up to 10^5, as compared with values of 10^4–10^7 estimated for Vulcanian eruptions.

Photographs of two typical laboratory flows are shown in Figure 3. The first (Fig. 3a–c) shows the evolution of a flow resulting from a short injection of a buoyant fluid, beginning at roughly 5 s into the experiment. The experimental source fluid was less dense than the ambient (960 kg m^{-3}) and consisted of a mixture of water, isopropyl alcohol and $<$10 μm diameter particles at 2 vol%. The flow began with a short momentum-driven phase reaching $<$0.1 m above the nozzle (Fig. 3a). In this particular case, the flow then formed two main lobes and continued to entrain ambient fluid and decelerate (Fig. 3b & c). Late in the flow development ($>$10 s after onset), the flow became more diffuse and the tail detached from the source (not shown). Other flows had greater source momentum, such that the momentum-dominated phase extended nearly to the top of the tank (Fig. 3d–f).

The time evolution of the vertical flow front velocity for a representative sample of the experimental data is shown in Figure 4. Experiments with both buoyancy and momentum, over a wide range of values, show a power law relationship such that vertical velocity, u, varies as t^{-1}, where t denotes the time measured from the point at which the flow front is first observed. There is greater scatter and some deviation from this relationship at both short and long times (not shown). At short times the flow is dominated by the initial geometry of release and vertical plume front velocity is independent of time. At long times the flow is affected by the presence of a free surface as it approaches the top of the tank, and in some cases late-stage flow-front velocities followed the trend of a purely buoyant thermal such that $u \approx t^{-1/2}$ (see below). The analysis that follows focuses primarily on the flow dynamics during the intermediate stages of the impulsive events when boundary effects are insignificant and both momentum and buoyancy are important.

Analysis

Here we develop a general scaling relationship for the rise rate of the experimental flows under conditions of varying buoyancy and momentum, using dimensional analysis to relate flow-front propagation and source conditions for all the experiments (see methods of Douglas 1969). Qualitative observations (Fig. 3) suggest that both buoyancy, B, (dimensions $L^4\ T^{-2}$) and momentum, M, (dimensions $L^4\ T^{-1}$) are likely to be important in controlling variation in the vertical rise velocity of the flow, u (dimensions $L\ T^{-1}$), with time, t. Here total buoyancy injected, B (per unit mass), is defined as the product of the total volume of solution released, V, and the reduced gravity, g'. Total momentum injected, M (per unit mass), is the product of the total volume, V, and the initial velocity, u_0. The volume of solution, V, also varies among experiments as the released volume is not limited (only the pressure of the release is set), but this is not an independent parameter as it is included in the definition of both B and M.

The functional form of the relationship $u = f(B,M,t)$ is sought. With four parameters consisting of two dimensions, $4 - 2 = 2$ dimensionless groups are expected. In the following analysis we choose to non-dimensionalize on the total buoyancy, B, although identical final results are obtained if total momentum is chosen as the non-dimensionalizing parameter. The appropriate dimensional scale for velocity is $B^{1/4}\ t^{-1/2}$, so the non-dimensional velocity scale for our flows is $ut^{1/2}/B^{1/4}$. The appropriate dimensional scale for momentum is Bt, so the non-dimensional momentum scale is M/Bt, which represents the source conditions. Therefore the propagation of the experimental flows is expected to follow the relationship

$$\frac{ut^{1/2}}{B^{1/4}} = f\left(\frac{M}{Bt}\right). \qquad (2)$$

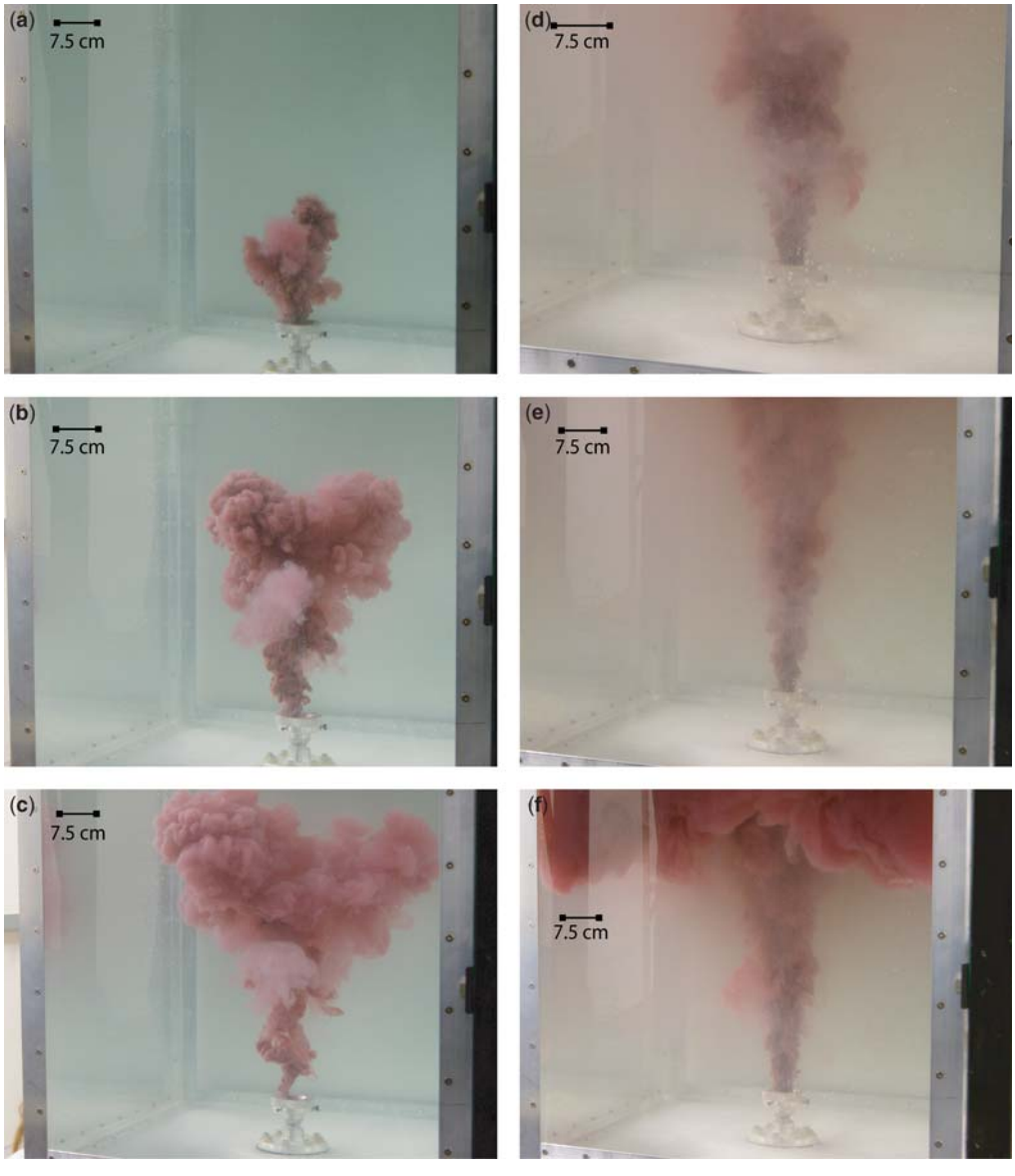

Fig. 3. (**a**–**c**) The release of a buoyant fluid ($\rho_{\mathrm{mix}} = 960$ kg m^{-3}) generated a buoyant plume, whose tail eventually detached from the vent. (**d**–**f**) The release of a buoyant fluid ($\rho_{\mathrm{mix}} = 960$ kg m^{-3}) where initial momentum dominated flow propagation until the flow front nearly reached the top of the tank.

The experimental data for flow propagation suggests that $u \approx t^{-1}$ (Fig. 4), so in order to be consistent with this observation, the appropriate functional form must be the power law

$$\frac{ut^{1/2}}{B^{1/4}} = k\left(\frac{M}{Bt}\right)^{1/2}. \tag{3}$$

This power law form represents a general relationship for finite-volume flows where both buoyancy and momentum are important. If the flow dynamics are not controlled by momentum, corresponding to the case where the exponent on the RHS is zero, the buoyant scaling for a thermal, $u \approx B^{1/4} t^{-1/2}$, is recovered (equivalent to that summarized in Turner 1973, pp. 186–189). If the flow dynamics are not controlled by buoyancy,

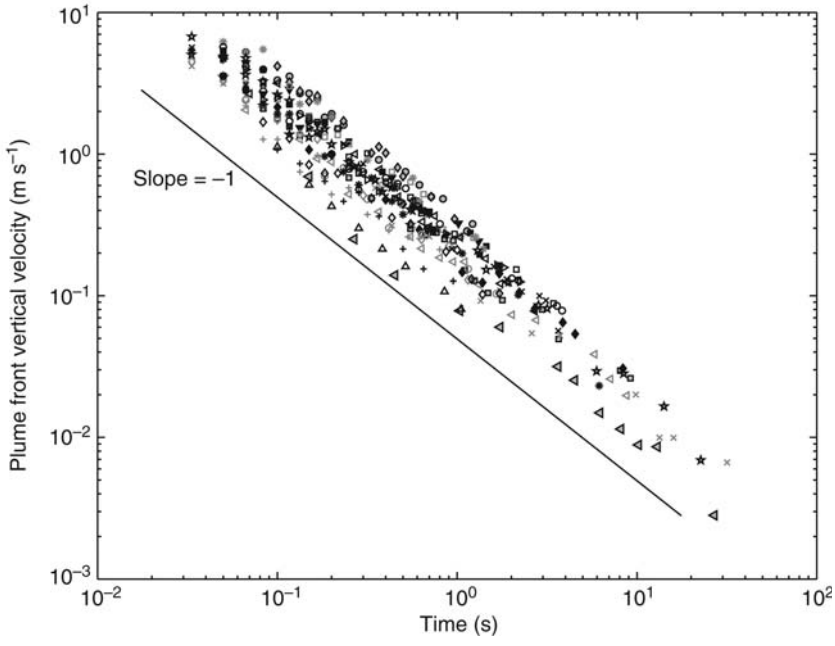

Fig. 4. Vertical velocity vs. time for a representative set of 20 experiments: u varies as t^{-1}, a regime for which both M and B control flow evolution. At short times, initial conditions and source geometry dominate the flow, and at long times the free surface affects the flow as it approaches the top of the tank (not shown). Uncertainty is $\pm 5\%$ for u, and ± 0.005 s for t.

corresponding to the case where the exponent on the RHS is $\frac{1}{4}$, the momentum scaling $u \approx M^{1/4}\, t^{-3/4}$ is recovered. The power law relationship between rise velocity u and time t is thus an indicator of the forces controlling the flow. In Figure 5 the time evolution of the flow front position is shown for flows where the buoyancy was zero (see Table 1). The form of the experimental data confirms the momentum scaling as appropriate in this case. The velocity of a finite-volume release controlled by both buoyancy and momentum decreases more rapidly than the cases where either buoyancy only or momentum only controls the flow. This observation is also made in the case of the analogous steady flow (forced plumes, Morton 1959).

The experimental data are plotted in Figure 6 in the form suggested by equation (3); only data from the region where flow front velocity varied as $u \approx t^{-1}$ (where both M and B are important) are included. The systematic experimental error was derived from measurements of mass flux injected to a precision of ± 0.001 kg s^{-1}, with precision of ± 0.005 s for the time, $\pm 5\%$ for the velocity, and negligible experimental error in determining the reduced gravity. Therefore the error bars on Figure 6 are comparable to the size of the symbols, which are given in Table 1. A satisfactory collapse of the experimental data is shown in Figure 6, illustrating that, for experiments in which both buoyancy and momentum are important, a universal relationship holds for a wide range of source and experimental conditions (Table 1), confirming the results of dimensional analysis (equation 3). The pre-multiplying constant, k, for the scaling relationship has a value of approximately 1, as determined from the curve fit to the data collapse (k is equivalent to the value of $ut^{1/2}/B^{1/4}$ when $(M/Bt)^{1/2} = 1$, Fig. 6).

Application to short-lived explosive eruptions

The non-dimensional scaling identified for our laboratory experiments is tested for several short-lived Vulcanian events in Figure 7. The literature sources of the field data are given in the caption. The Vulcanian eruption data, albeit sparse, collapses to a single trend, coincident with that of the experimental data. Data from Vulcanian eruptions sometimes required smoothing (e.g. data from Santiaguito volcano presented in Fig. 8). The large fluctuations in Figure 8a are interpreted to represent turbulent variations in flow front propagation, whereas the

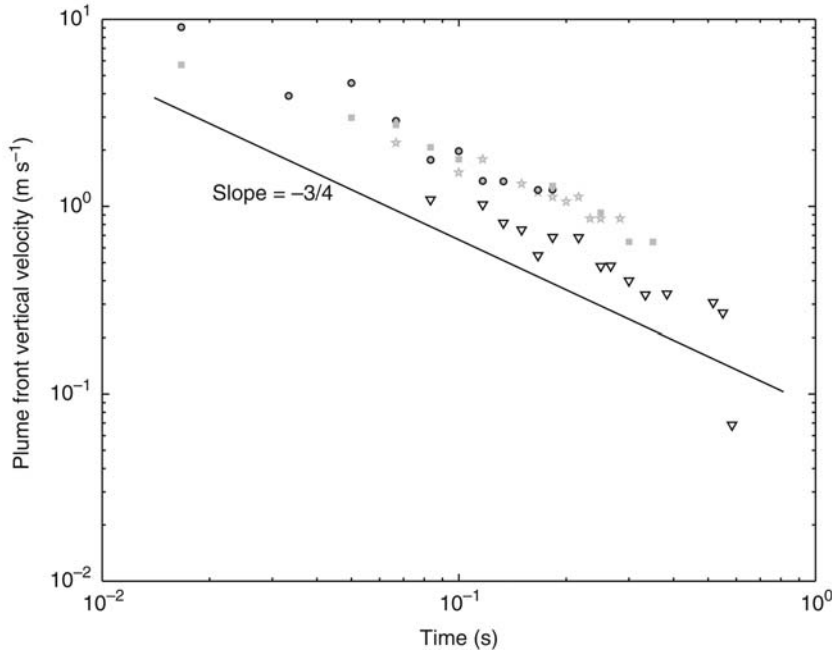

Fig. 5. Vertical velocity v. time for a representative set of four experiments: u varies as $t^{-3/4}$, a regime for which only M controls flow evolution because the injected fluid is neutrally buoyant. At short times, initial conditions and source geometry dominate the flow, and at long times the free surface affects the flow as it approaches the top of the tank (not shown). Uncertainty is $\pm 5\%$ for u, and ± 0.005 s for t.

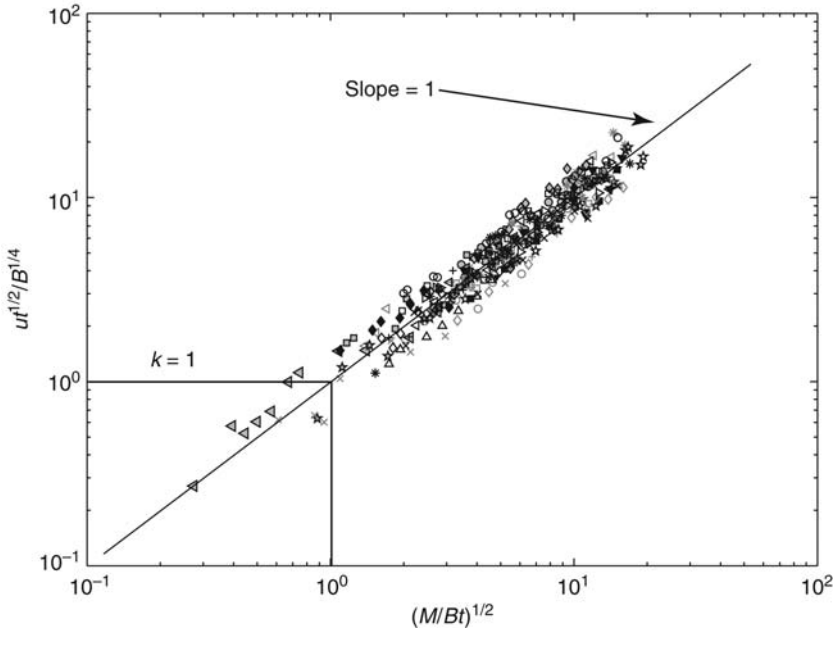

Fig. 6. All experimental data in terms of non-dimensional velocity and momentum (equation 3), where $k = 1$, as determined by the value of $ut^{1/2}/B^{1/4}$ where $(M/Bt)^{1/2} = 1$. The slope of the line is 1 and simply indicates that the relationship between $ut^{1/2}/B^{1/4}$ and $(M/Bt)^{1/2}$ is linear. Uncertainty is represented by the size of the symbols and primarily reflects uncertainty in u ($\pm 5\%$) and t (± 0.005 s). The details of each experiment are listed in Table 1.

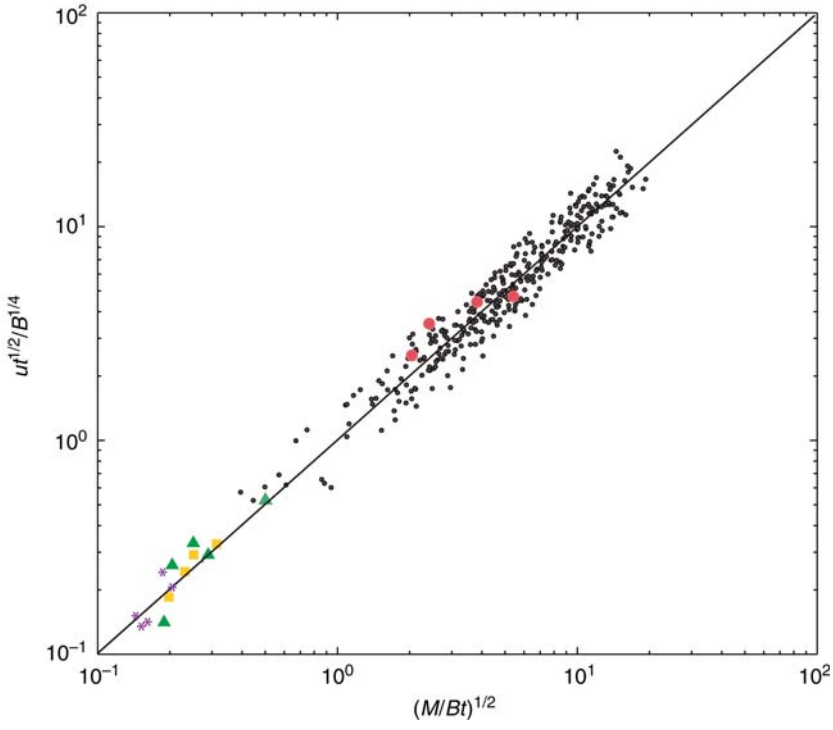

Fig. 7. All experimental data (black dots) and four Vulcanian eruptions (other symbols) plotted in the form suggested by equation (3). The Vulcanian data are for: the 20 February 1990 eruption of Lascar volcano in Chile (circles), with velocity values from Sparks *et al.* (1997, p. 132, fig. 5.11), DRE erupted from Sparks *et al.* (1997, p. 134, fig. 5.14, eruption rate times duration) and mixture density assumed to be 1 kg m^{-3} (as suggested by Sparks & Wilson 1982); the 7 August 1997 eruption of the Soufrière Hills volcano, Montserrat (squares), with velocity values from Clarke *et al.* (2002), DRE erupted from Druitt *et al.* (2002) and mixture density of 20 kg m^{-3} from Formenti *et al.* (2003, fig. 11); the 6 October 1997 eruption of the Soufrière Hills volcano, Montserrat (*), with velocity values from Formenti *et al.* (2003), DRE erupted from Druitt *et al.* (2002) and mixture density 20 kg m^{-3} from (Formenti *et al.* 2003, fig. 11); and the 22 July 1980 eruption of Mount St Helens, USA (triangles), with velocity values from Hoblitt (1986, timed photographs), an assumed DRE erupted of 5×10^5 m^3 and an assumed mixture density of 20 kg m^{-3}, equal to estimates for collapsing fountains at SHV.

desired velocity is the mean velocity. To smooth the fluctuations, plume front height was initially plotted against time and fitted with a polynomial and then differentiated to estimate plume front vertical velocity as a function of time (compare Fig. 8b against the raw data in Fig. 8a). However, in the data presented here, we opted for a smoothing-by-eye technique in which outliers were simply eliminated (Fig. 8c), resulting in the same general trends. The two non-dimensional groupings defined in the previous section capture the controlling trend in both the laboratory flows and Vulcanian eruptions (Fig. 7).

We next solve equation (3) for total fluid volume injected, yielding

$$V = \frac{u^4 t^4 g'}{k^4 u_0^2}. \qquad (4)$$

Equation (4) can be used to estimate the solid mass erupted as a function of time, simply by multiplying the whole equation by the density of the gas–pyroclast mixture, ρ_{mix}. The potential utility of equation (4) will be demonstrated by applying it to the well-documented 7 August 1997, Vulcanian eruption at Soufrière Hills volcano (SHV), Montserrat (Druitt *et al.* 2002). A value of $g' = 150$ m s^{-2} was used, which corresponds to $\rho_{\mathrm{mix}} = 20$ kg m^{-3}, consistent with asymptotic values estimated by Formenti *et al.* (2003, fig. 11) for several Vulcanian events at SHV in 1997. The results from equation (4) are shown in Figure 9, where the total mass erupted reaches a constant value of approximately 10^9 kg (5×10^5 m^3 DRE) after about 10 s, providing an estimate of eruption magnitude. The slope and duration of the trend preceding this plateau offer an estimate of vent mass flow rate and duration of the

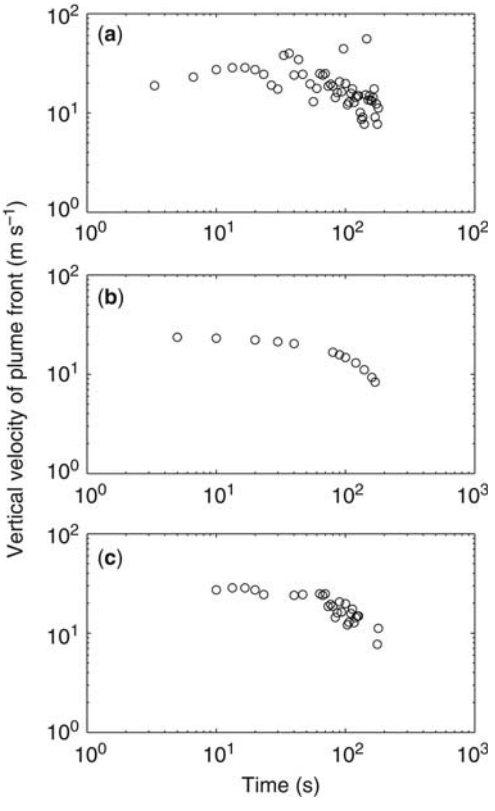

Fig. 8. Data acquired from video analysis of a Vulcanian eruption at Santiaguito volcano, Guatemala, in January of 2005. (**a**) Vertical plume front velocity, u, v. time, t, unsmoothed data; (**b**) vertical plume front velocity as function of time, where velocity was obtained by differentiating a polynomial fit of plume front height v. time; (**c**) smoothed vertical plume front velocity v. time, where large turbulent velocity fluctuations were omitted manually.

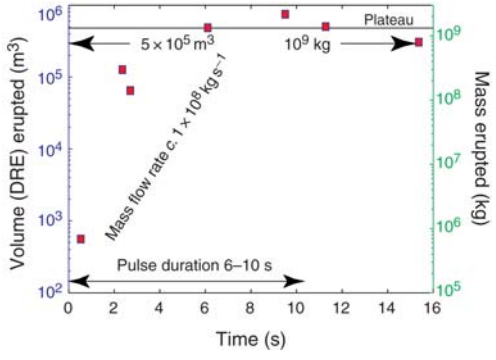

Fig. 9. Calculation of mass and volume DRE erupted for the 7 August 1997 Vulcanian eruption of Soufrière Hills volcano, based on the empirical relationship of equation (4), where $k = 1$. The slope over the first 10 s indicates a vent mass flow rate of 10^8 kg s^{-1}. Estimated total mass and DRE erupted are 10^9 kg and 5×10^5 m^3 DRE, respectively, where equivalent DRE density is 2500 kg m^{-3}.

eruptive pulse; for this SHV event, we calculate a mass flux of roughly 10^8 kg s^{-1}, lasting approximately10 s. The calculated total mass erupted is slightly larger than the average size of the 1997 Vulcanian events at SHV (3×10^5 m^3 DRE, 7.5×10^8 kg), estimated by Druitt *et al.* (2002) from deposit mapping and column height. Our estimate is consistent with the fact that the 7 August event produced a higher-than-average column (14 km compared with the average 10 km), suggesting that its mass erupted may have been slightly higher than average. Frequency analysis of seismic records from the 7 August and similar events suggests that the main pulse lasted 10–20 s (Druitt *et al.* 2002; our unpublished seismic analysis of the 7 August event).

Discussion

We have identified a universal scaling relationship for the dynamics of Vulcanian eruptions and finite-volume (impulsive) releases of fluid controlled by both momentum and buoyancy. These flows show a greater rate of deceleration ($u \approx t^{-1}$) than either purely buoyant ($u \approx t^{-1/2}$) or purely momentum-driven ($u \approx t^{-3/4}$) flows. These relative rates of deceleration are consistent with the analogous steady cases (a forced plume compared to a pure plume or a jet; Turner 1973; Rajaratnam 1976; Sparks *et al.* 1997). The scaling collapses the experimental data regardless of whether the initial buoyancy is positive or negative because the laboratory observations cover the region where initial momentum has a greater effect than initial buoyancy. The resulting scaling relationships show that flow-front propagation of Vulcanian events provides all the evidence required to estimate vent conditions (buoyancy and momentum released). However, when converting buoyancy and momentum released to mass erupted, reliable and precise estimates of vent particle concentration (and therefore erupted mixture density) are required. Unfortunately such values are difficult to constrain and could vary widely from event to event. This uncertainty should motivate development of independent techniques of measuring or estimating initial mixture density.

The difference in compressibility between laboratory and field conditions should be considered carefully and is discussed below. Applying a well-validated numerical model (CFDLIB) and carefully

examining their velocity data, Formenti *et al.* (2003) show that, for Vulcanian eruptions at Soufrière Hills volcano, Montserrat, pressure inside individual jets adjusts to atmospheric pressure within 50 m above the vent (within *c.* 2 vent diameters), and initially supersonic flows decelerate to subsonic conditions over similar distances. Their finding is reasonably consistent with other field observations (velocity data in Fig. 7), and with relationships based on underexpanded supersonic jet experiments (Yüceil & Ötügen 2002), which allow the location and characteristics of the virtual source (the point at which the flow becomes pressure-balanced) to be calculated from physical vent conditions. According to the study, an underexpanded jet reaches ambient pressure at some finite distance from the vent (the expansion region), beyond which the jet behaves as an ordinary pressure-balanced jet and therefore does not go through any additional pressure adjustments.

Applying, with caution, the relationships derived for steady, supersonic, ideal-gas jets (Yüceil & Ötügen 2002) and assuming eruption pressures ranging from 1 to 10 MPa (Chojnicki *et al.* 2006), we estimate virtual source characteristics of typical Vulcanian eruptions. The estimates depend strongly on input parameters which can be difficult to constrain. However, even for the highest eruption pressures and end-member values of fluid properties (sound speed, $a = 10$ m s^{-1}; ratio of specific heats, γ approaching 1), the calculated distance from physical vent to virtual source is not more than 700 m, and in most cases does not significantly exceed 100 m. The virtual diameter in the most extreme cases is much larger than physical vent diameter (by a factor of 8), but is changed by only a factor of 2 at low exit pressures. The velocity at the virtual source is only slightly larger than it is at the actual vent (increase by a factor of *c.* 1.1). On the other hand, mixture density appears to be strongly affected by expansion of water vapour between the physical and virtual vents, with mixture density decreasing by up to a factor of 70 for the highest exit pressures. Given that Vulcanian eruption velocities generally decay to subsonic velocities quickly, and that most data is taken from points greater than one hundred metres from the physical vent (see literature sources of Fig. 7), we assert that the data generally represent the pressure-balanced, subsonic portion of the flow. These relationships also suggests that source conditions derived from our relationships (equations 3 and 4) apply to a virtual source, rather than a physical vent, and that this distinction may be most significant for very high eruption pressures (10 MPa), representing relatively rare Vulcanian events. We also suggest that future field measurements of initial mixture density consider this distinction.

Conclusions and recommendations

We develop a robust scaling relationship (equations 3 & 4, Figs 6 & 7) that captures the dynamics of the propagation of short-lived laboratory experiments and several observed Vulcanian eruptions where both momentum and buoyancy may be important to flow propagation. The relationship was successfully applied to the well-documented event of 7 August 1997 at Soufrière Hills volcano, Montserrat, in order to demonstrate how the analysis can be used to estimate the time-varying vent mass flux and total mass erupted for a Vulcanian eruption (which can not be measured directly) from the vertical flow-front velocity (Fig. 9). The scaling relationship on which this estimate is based holds over a wide range of initial conditions, so the method is robust and does not depend on whether the flow is positively buoyant or purely momentum driven.

In order to better understand Vulcanian eruption dynamics, we strongly recommend more detailed field documentation of short-lived explosive eruptions. Field studies, when possible, should measure plume vertical velocity as a function of time, use deposits to constrain total mass erupted for individual events, and use seismic signals to estimate pulse duration (e.g. Druitt *et al.* 2002). Vent particle concentration (and therefore erupted mixture density) is difficult to constrain and could vary widely from event to event. However, if both time-variant plume front vertical velocity and total mass erupted are independently measured, the relationships presented here for real eruptions (equation 4) can be used to constrain vent (virtual source) particle concentration. Novel ways to directly measure particle concentration and mixture density at the vent would greatly improve our understanding of impulsive explosive eruptions.

We gratefully acknowledge helpful discussions with H. J. Fernando, A. J. Hogg, laboratory assistance from C. Skiba, and financial support from NSF EAR 0541925. This manuscript was improved by the insightful reviews by M. T. Guðmundsson & B. Zimanowski as well as suggestions from the editors, in particular by Guðrún Larsen.

References

CAREY, S. & SIGURDSSON, H. 1987. Temporal variations in column height and magma discharge rate during the 79 A.D. eruption of Vesuvius. *Geological Society of America Bulletin*, **99**, 303–314.

CHOJNICKI, K., CLARKE, A. B. & PHILLIPS, J. C. 2006. A shock-tube investigation of the dynamics of gas-particle mixtures: implications for explosive volcanic eruptions. *Geophysical Research Letters*, **33**, L15309, doi:10.1029/2006FL026414.

CLARKE, A. B., NERI, A., MACEDONIO, G., VOIGHT, B. & DRUITT, T. H. 2002. Computational modeling of the transient dynamics of the August 1997 Vulcanian explosions at Soufrière Hills volcano, Montserrat: influence of initial conduit conditions on near-vent pyroclastic dispersal. *Journal of the Geological Society, London, Memoir*, **21**, 319–348.

COOKMAN, J. L., METZGER, J. M., FLEMINGS, P. B. & SLINGERLAND, R. L. 1997. A numerical model of sedimentation from suspension in a buoyant plume. *Eos, Transactions, American Geophysical Union*, **78**, Fall Meeting Supplement, 276.

DI MURO, A., NERI, A. & ROSI, M. 2004. Contemporaneous convective and collapsing eruptive dynamics: The transitional regime of explosive eruptions. *Geophysical Research Letters*, **31**, L10607; doi:10.1029/2004GL019709.

DOUGLAS, J. F. 1969. *An Introduction to Dimensional Analysis for Engineers*. Pitman, London.

DRUITT, T. H. & YOUNG, S. R. 2002. Episodes of cyclic Vulcanian explosive activity with fountain collapse at Soufrière Hills volcano, Montserrat. *In*: DRUITT, T. H. & KOKELAAR, B. P. (eds) *The Eruption of Soufrière Hills Volcano, Montserrat, from 1995 to 1999*. Geological Society, London, Memoirs, **21**, 281–306.

FAGENTS, S. A. & WILSON, L. 1993. Explosive volcanic eruptions – VII. The ranges of pyroclasts ejected in transient volcanic explosions. *Geophysical Journal International*, **113**, 359–370.

FORMENTI, Y., DRUITT, T. H. & KELFOUN, K. 2003. Characterization of the 1997 Vulcanian explosions of Soufrière Hills Volcano, Montserrat, by video analysis. *Bulletin of Volcanology*, **65**, 587–605.

HOBLITT, R. 1986. *Observations of the Eruptions of July 22 and August 7, 1980, at Mount St. Helens, Washington*. United States Geological Survey Professional Papers, **1335**.

HOUGHTON, B. F., WILSON, C. J. N., FIERSTEIN, J. & HILDRETH, W. 2004. Complex proximal deposition during the Plinian eruptions of 1912 at Novarupta, Alaska. *Bulletin of Volcanology*, **66**, 95–133.

ISHIHARA, K. 1985. Dynamical analysis of volcanic explosion. *Journal of Geodynamics*, **3**, 327–349.

JOHNSON, J. B., HARRIS, A. J. L., SAHETAPY-ENGEL, S. T. M., WOLF, R. & ROSE, W. I. 2004. Explosion dynamics of pyroclastic eruptions at Santiaguito Volcano. *Geophysical Research Letters*, **31**, L06610; doi:10.1029/2003GL019079.

KAMINSKI, E., TAIT, S. & CARAZZO, G. 2005. Turbulent entrainment in jets with arbitrary buoyancy. *Journal of Fluid Mechanics*, **526**, 361–376.

LEE, K., LEE, C. & JOO, Y. 2004. Application technique of particle image velocimetry and entropy analysis to investigate spray structure for gasoline direct injection injector. *Measurements in Science and Technology*, **14**, 953–964.

MORRISSEY, M. M. & MASTIN, L. G. 2000. Vulcanian Eruptions. *In*: SIGURDSSON, H. (eds) *Encyclopedia of Volcanoes*. Academic Press, San Diego, CA, 463–475.

MORTON, B. R. 1959. Forced plumes. *Journal of Fluid Mechanics*, **5**, 151–163.

MORTON, B. R., TAYLOR, G. I. & TURNER, J. S. 1956. Turbulent gravitational convection from maintained and instantaneous sources. *Philosophical Transactions of the Royal Society of London A*, **234**, 1–23.

NAIRN, I. A. 1976. Atmospheric shock waves and condensation clouds from Ngaurhoe explosive eruptions. *Nature*, **259**, 190–192.

NAIRN, I. A. & SELF, S. 1978. Explosive eruptions and pyroclastic avalanches from Ngauruhoe in February 1975. *Journal of Volcanology and Geothermal Research*, **3**, 39–60.

RAJARATNAM, N. 1976. *Turbulent Jets*. Elsevier, Amsterdam.

ROSE, W. I. 1980. Gas and hydrogen isotopic analyses of volcanic eruptions clouds in Guatemala sampled by aircraft. *Journal of Volcanology and Geothermal Research*, **7**, 1–10.

SCOTT, W. E., HOBLITT, R. P., TORRES, R. C., SELF, S., MARTINEZ, M. L. & NILLOS, T. JR. 1996. Pyroclastic flows of the June 15, 1991, climactic eruption of Mount Pinatubo. *In*: NEWHALL, C. G. & PUNONGBAYAN, R. S. (eds) *Fire and Mud: Eruptions and Lahars of Mount Pinatubo, Philippines*. University of Washington Press, Seattle, WA, 545–570.

SELF, S., WILSON, L. & NAIRN, I. A. 1979. Vulcanian eruption mechanisms. *Nature*, **277**, 440–443.

SPARKS, R. S. J. & WILSON, L. 1982. Explosive volcanic eruptions – V. Observations of plume dynamics during the 1979 Soufrière eruptions, St. Vincent. *Geophysical Journal of the Royal Astronomical Society*, **69**, 551–570.

SPARKS, R. S. J., BURSIK, M. I., CAREY, S. N., GILBERT, J. S., GLAZE, L. S., SIGGURDSSON, H. & WOODS, A. 1997. *Volcanic Plumes*. John Wiley & Sons, New York.

STIX, J., TORRES, R. C., NARVÁEZ, L., CORTÉS, P., RAIGOSA, J., GÓMEZ, D. & CASTONGUAY, R. 1997. A model of Vulcanian eruptions at Galeras volcano, Colombia. *Journal of Volcanology and Geothermal Research*, **77**, 285–303.

SUDARIKOV, S. M. & ROUMIANTSEV, A. B. 2000. Structure of hydrothermal plumes at the Logatchev vent field, 14 degrees 45′N, Mid-Atlantic Ridge; evidence from geochemical and geophysical data. *Journal of Volcanology and Geothermal Research*, **101**, 245–252.

TURNER, J. S. 1966. Jets and plumes with negative or reversing buoyancy. *Journal of Fluid Mechanics*, **26**, 779–792.

TURNER, J. S. 1973. *Buoyancy Effects in Fluids*. Cambridge University Press, New York.

WAITT, R. B., MASTIN, L. G. & MILLER, T. P. 1995. Ballistic showers during Crater Peak eruptions of Mount Spurr Volcano, summer 1992. *United States Geological Survey Bulletin*, **2139**, 89–106.

WILSON, L., SPARKS, R. S. J. & WALKER, G. P. L. 1980. Explosive Volcanic Eruptions IV. The control of magma properties and conduit geometry on eruption column behaviour. *Geophysical Journal of the Royal Astronomical Society*, **63**, 117–148.

WOHLETZ, K. H. 2001. Pyroclastic surges and compressible two-phase flow. *In*: FREUNDT, A. & ROSI, M. (eds) *From Magma to Tephra*. Elsevier, Amsterdam, 247–312.

WOODS, A. W. 1995. A model of vulcanian explosions. *Nuclear Engineering and Design*, **155**, 345–357.

YÜCEIL, K. B. & ÖTÜGEN, M. V. 2002. Scaling parameters for underexpanded supersonic jets. *Physics of Fluids*, **14**, 4206–4215.